Spatiotemporal Behavior Induced by Differential Diffusion in Landolt Systems

ARTICLE *in* THE JOURNAL OF PHYSICAL CHEMISTRY A · OCTOBER 2014

Impact Factor: 2.69 · DOI: 10.1021/jp508836p · Source: PubMed

1 AUTHOR:

Istvan Szalai
Eötvös Loránd University
44 PUBLICATIONS **611** CITATIONS

SEE PROFILE

THE JOURNAL OF PHYSICAL CHEMISTRY A

Article

pubs.acs.org/JPCA

Spatiotemporal Behavior Induced by Differential Diffusion in Landolt Systems

István Szalai*

Institute of Chemistry, Eötvös University, Budapest, Hungary 1117

ABSTRACT: The spatiotemporal dynamics of Landolt type reactions, for instance reactions between sulfite ions and strong oxidants, performed in a medium fed by the diffusion from a boundary is investigated numerically by using a simple general reaction scheme. In these conditions, the model can generate various spatiotemporal phenomena, e.g., spatial bistability, simple and complex oscillations, birhythmicity, and chaos, even though in a spatially homogeneous open reactor only steady-state bistability can develop. The model consists of two reactions, a protonation equilibrium of the reductant and an oxidation step that is autoactivated by hydrogen ions. The rich dynamics is the result of two factors: (i) long-range activation, through the rapidly diffusing hydrogen ions, (ii) the presence of two parallel autocatalytic pathways. Long range activation provides the necessary negative feedback, whereas the dual nature of the autocatalysis leads to the appearance of two different oscillatory modes. The presence of a second-order term in the rate law of the autocatalytic reaction is linked to a large amplitude oscillations that affect the system as a whole, whereas the third-order one gives rise to localized front oscillations. The complex phenomena, like mixed mode and chaotic oscillations are observed at the meeting of these different oscillatory modes.

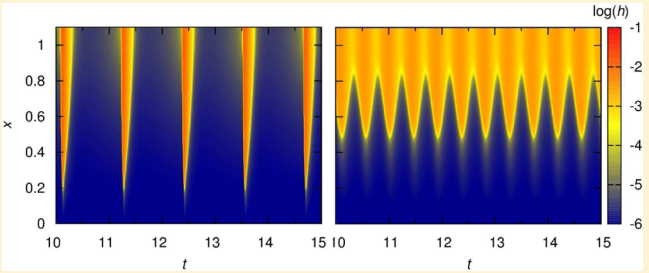

INTRODUCTION

Pattern formation in chemical reaction−diffusion systems with positive and negative feedback is the prototype of non-equilibrium self-organization.[1] Although the detailed mechanisms of these reactions are usually complicated, relatively simple skeleton models can be effectively used to reproduce the essential properties of the emerging phenomena. Besides, the classical examples, e.g., the Belousov−Zhabotinsky and the chlorite−iodide−malonic acid reaction families, the hydrogen ion autocatalytic systems are the ones most often used to study such phenomena. From a mechanistic point of view, there are two different classes of these reactions according to the acid−base character of the substrate. The first one includes the oxidation of an unprotonated compound, like in the versatile chlorite−tetrathionate (CT) reaction.[2] In this case water is the source of the hydrogen ions. The second type is based on the oxidation of a weak acid−base pair, where the protonated form reacts faster than the unprotonated one and the product is a strong acid. Consequently, as the hydrogen ion concentration rises during the reaction, the overall process is accelerated. In this type of reaction the amount of the hydrogen ions produced by the reaction is determined by the initial amount of the protonated form of the substrate. Among others, the reactions between sulfite ions and oxidants like iodate (IS),[3] bromate (BS),[4] or hydrogen peroxide (HPS)[5] belong to this later category. We call this class Landolt type systems.

A basic phenomenon of the autocatalytic reaction−diffusion systems fed by the diffusion of reactants from a boundary is spatial bistability.[6,7] This corresponds to the coexistence of two steady states, characterized by different spatial concentration distributions. Spatial bistability has been observed in both groups of the hydrogen ion autocatalytic reactions.[8−11] A standard device to study spatiotemporal chemical structures is called open one-side-fed reactor (OSFR), in which an inert hydrogel is in contact along one of its surfaces with a content of a continuous stirred tank reactor (CSTR). This configuration allows us to maintain the gel content far from equilibrium and the gel medium avoids the convective motion of the fluid. The CSTR serves as a reservoir of a fresh mixture of reactants; thus it is kept in a low extent of reaction ($\xi \sim 0$) state (F_{cstr}). The reactions can take place mainly in the gel, where ξ increases along the normal of the feeding surface (hereafter called the x axis). The steady state, at which ξ is low even at the furthermost point of the gel from the feeding surface, is called the F state of the gel. In the vicinity of the feeding surface, ξ is necessarily low, as in the CSTR, in the depth of the gel, depending on the conditions (e.g., on the thickness of the gel (L_x)) the autocatalytic process can eventuate. Consequently, a chemical front can develop in the depth of the gel that connects the $\xi \sim 0$ state at $x = 0$ with the $\xi \sim 1$ state at $x = L_x$. This is called the M state of the gel content. Spatial bistability refers to the coexistence of the F and M states for the same environmental (CSTR) conditions. Theoretical studies based on a cubic autocatalytic model have pointed out that the appearance of spatial bistability is the consequence of the Dirichlet boundary condition at the gel/CSTR surface and the finite thickness of the gel.[7] In hydrogen ion autocatalytic systems, the F state is characterized with high pH all along the x axes, whereas at the

Received: September 1, 2014
Revised: October 21, 2014
Published: October 22, 2014

M state the pH is high at $x = 0$ and turns sharply to a several units lower value in the depth of the gel.

The diffusive nature of the matter exchange between the CSTR content and the gel opens the door to new instabilities. When the autocatalytic species diffuses faster than the other components, which is naturally the case in hydrogen ion autocatalytic reactions, this long-range activation can induce an oscillatory instability. This has been experimentally first observed in the CT reaction, where beyond a control parameter threshold, the front position of the M state moves back and forth along the x axes.[8,12] This type of oscillatory state is referred to as M′. The study of this bifurcation on simple cubic autocatalytic models has shown that the oscillations emerge from a Hopf bifurcation when the ratio of the diffusion coefficient of the reactant and the autocatalyst $\delta = D_{\text{reagent}}/D_{\text{autocatalyst}} \lesssim 1/5$.[13,14] This prerequisite is fulfilled in aqueous phase hydrogen ion autocatalytic reactions if only strong electrolytes are in the reaction mixture. However, the effective diffusivity of hydrogen ions is influenced by weak acid/base type electrolytes. As the protonation equilibrium of a weak acid is the crucial point in the mechanism of the Landolt type systems, the development of long-range activation oscillations in this case is not straightforward. Until now, these phenomena have been observed only in the IS, and not in the BS and HPS reactions.[9−11] The reason for the different behaviors of these analogous reactions has not been clarified yet. Furthermore, the experimentally observed oscillatory dynamics of the IS system differ significantly from that of the CT reaction. In the IS reaction two types of spatiotemporal oscillations have been experimentally reported. Besides, the M′ type, a second type of oscillations can develop, at which nearly all along the x axes the state of the gel content changes periodically between small and large ξ values, thus between high and low pH. Numerical simulations based on a detailed kinetic model could reproduce the observed phenomena and show that both types of oscillations are the consequence of long-range activation.[15] Long range activation could be quenched by adding a low mobility weak electrolyte to the reaction mixture, which slows down the mobility of the hydrogen ions. This quenching of oscillations develop differently in the CT and in the IS reaction.[16,17] The oscillation is longer lived at larger values of thickness than at smaller ones in the CT, and just the opposite dependence has been found in the IS system. This reveals again the important differences between the two classes of the hydrogen ion autocatalytic systems. Recently, it has also been shown that a similar mechanism can produce spatiotemporal oscillations in enzymatic reactions with bell-shaped pH-rate characteristics.[18]

Here, we numerically study the spatiotemporal dynamics of the Landolt type systems in an OSFR, by using a general kinetic model. This model has been found to be capable of accounting for the clock behavior observed in the oxidations of sulfite ions by different oxidants,[19] and for their respective CSTR dynamics. We show that the simple chemistry of this model in the presence of long-range activation results in a quite complex spatiotemporal dynamics including spatial bistability, oscillations, birhythmicity, mixed mode, and chaotic oscillations. We highlight the respective roles played by the kinetic parameters of the oxidation step and by differential diffusion.

THE MODEL

The Rábai model[20] of the autocatalytic oxidation of a weak acid includes a protonation equilibrium (R1) of the substrate (A^-) and oxidation of the protonated form (HA) by the strong oxidant (B) in reaction R2:

$$A^- + H^+ \rightleftharpoons HA \tag{R1}$$

$$HA + B \xrightarrow{H^+} H^+ + P \tag{R2}$$

We skipped the inclusion of the water dissociation equilibrium, because it does not affect significantly the bistability presented in Figure 1. The most commonly used substrate is the sulfite ion and the typical oxidants are iodate, bromate, and hydrogen peroxide, and the experimentally observed rate law of (R2) can be written in a common form: $v_2 = (k_2[H^+] + k_2')[HA][B]$, independently from the chemical nature of B. That means that the system consists of two parallel autocatalytic processes, e.g., the oxidations of HSO_3^- and H_2SO_3. By using this rate law, on can describe the CSTR dynamics of the model by the following set of equations:

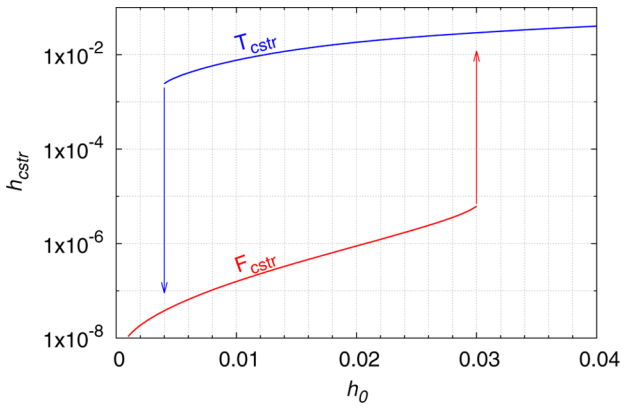

Figure 1. Bistability of the CSTR content at $\kappa_2 = 5 \times 10^5$, $\kappa_2' = 50$, $\kappa_1 = 5 \times 10^{10}$, $\kappa_{-1} = 5 \times 10^5$, and $b_0 = 1.5$.

$$\frac{d[A^-]_{cstr}}{dt} = -k_1[A^-]_{cstr}[H^+]_{cstr} + k_{-1}[HA]_{cstr} + k_0([A^-]_0 - [A^-]_{cstr}) \tag{1}$$

$$\frac{d[HA]_{cstr}}{dt} = k_1[A^-]_{cstr}[H^+]_{cstr} - k_{-1}[HA]_{cstr} - (k_2[H^+]_{cstr} + k_2')[HA]_{cstr}[B]_{cstr} - k_0[HA]_{cstr} \tag{2}$$

$$\frac{d[H^+]_{cstr}}{dt} = -k_1[A^-]_{cstr}[H^+]_{cstr} + k_{-1}[HA]_{cstr} + (k_2[H^+]_{cstr} + k_2')[HA]_{cstr}[B]_{cstr} + k_0([H^+]_0 - [H^+]_{cstr}) \tag{3}$$

$$\frac{d[B]_{cstr}}{dt} = -(k_2[H^+]_{cstr} + k_2')[HA]_{cstr}[B]_{cstr} + k_0([B]_0 - [B]_{cstr}) \tag{4}$$

where $[\ ]_{cstr}$ and $[\ ]_0$ are concentrations in the CSTR and in the input feed, respectively. The feedback of the gel content on the state of the CSTR is neglected, because in the typical experiment the volume of the CSTR is much larger than that of the gel. The 1D dynamics of the gel content, along the axial direction (x) is governed by the following set of equations:

dx.doi.org/10.1021/jp508836p | J. Phys. Chem. A 2014, 118, 10699−10705

$$\partial_t[A^-] = -k_1[A^-][H^+] + k_{-1}[HA] + D_{A^-}\partial_x^2[A^-] \quad (5)$$

$$\partial_t[HA] = k_1[A^-][H^+] - k_{-1}[HA] - (k_2[H^+] + k_2')[HA][B] + D_{HA}\partial_x^2[HA] \quad (6)$$

$$\partial_t[H^+] = -k_1[A^-][H^+] + k_{-1}[HA] + (k_2[H^+] + k_2')[HA][B] + D_{H^+}\partial_x^2[H^+] \quad (7)$$

$$\partial_t[B] = -(k_2[H^+] + k_2')[HA][B] + D_B\partial_x^2[B] \quad (8)$$

with Dirichlet boundary conditions at the gel/CSTR surface, e.g., $[A^-]_{(x=0)} = [A^-]_{cstr}$, and no flux boundary conditions at the gel/impermeable wall surfaces, e.g., $(\partial_x[A^-])_{(x=L_x)} = 0$.

With the dimensionless variables $a_{cstr} = [A^-]_{cstr}/[A^-]_0$, $a^h_{cstr} = [HA]_{cstr}/[A^-]$, $h_{cstr} = [H^+]_{cstr}/[A^-]_0$, $b_{cstr} = [B]_{cstr}/[A^-]_0$, $a = [A^-]/[A^-]_0$, $a^h = [HA]/[A^-]_0$, $h = [H^+]/[A^-]_0$, and $b = [B]/[A^-]_0$ eqs 1−4 and 5−8 are written as

CSTR content:

$$\dot{a}_{cstr} = -\kappa_1 a_{cstr} h_{cstr} + \kappa_{-1} a^h_{cstr} + 1 - a_{cstr} \quad (9)$$

$$\dot{a}^h_{cstr} = \kappa_1 a_{cstr} h_{cstr} - \kappa_{-1} a^h_{cstr} - (\kappa_2 h_{cstr} + \kappa_2') a^h_{cstr} b_{cstr} - a^h_{cstr} \quad (10)$$

$$\dot{h}_{cstr} = -\kappa_1 a_{cstr} h_{cstr} + \kappa_{-1} a^h_{cstr} + (\kappa_2 h_{cstr} + \kappa_2') a^h_{cstr} b_{cstr} + h_0 - h_{cstr} \quad (11)$$

$$\dot{b}_{cstr} = -(\kappa_2 h_{cstr} + \kappa_2') a^h_{cstr} b_{cstr} + b_0 - b_{cstr} \quad (12)$$

gel content:

$$\partial_t a = -\kappa_1 a h + \kappa_{-1} a^h + \partial_x^2 a \quad (13)$$

$$\partial_t a^h = \kappa_1 a h - \kappa_{-1} a^h - (\kappa_2 h + \kappa_2') a^h b + \partial_x^2 a^h \quad (14)$$

$$\partial_t h = -\kappa_1 a h + \kappa_{-1} a^h + (\kappa_2 h + \kappa_2') a^h b + \frac{1}{\delta}\partial_x^2 h \quad (15)$$

$$\partial_t b = -(\kappa_2 h + \kappa_2') a^h b + \partial_x^2 b \quad (16)$$

The dimensionless space and time coordinates are scaled by $(k_0/D)^{1/2}$ and k_0, respectively. The parameters are defined as $\kappa_1 = k_1[A^-]_0/k_0$, $\kappa_{-1} = k_{-1}/k_0$, $\kappa_2 = k_2[A^-]_0^2/k_0$ $\kappa_2' = k_2'[A^-]_0/k_0$, $h_0 = [H^+]_0/[A^-]_0$, and $b_0 = [B]_0/[A^-]_0$. The diffusion coefficients are set to be equal for all species ($D_{A^-} = D_{HA} = D_B = D$) except for the hydrogen ions, where $D_{H^+} = D/\delta$. Hereafter, ∂_t and ∂_x denote the derivatives according to the dimensionless time and space coordinates, respectively.

The values of κ_1, κ_{-1}, and b_0 are set to 5×10^{10}, 5×10^5, and 1.5, respectively, which are calculated by using the following kinetic parameter values for the protonation of sulfite ions ($k_1 = 10^{10}$ mol^{-1} dm^3 s^{-1}, $k_{-1} = 10^3$ s^{-1}) and a set of typical experimental conditions, e.g., $k_0 = 2 \times 10^{-3}$ s^{-1}, $[A^-]_0 = 10$ mM, $[B]_0 = 15$ mM. For compatibility with the experiments[9−11,17] we use h_0, $l_x = L_x(k_0/D)^{1/2}$, and δ as control parameters.

The partial differential equations were discretized with a standard second-order finite difference scheme on a 200 mesh. The resulting systems were solved by the SUNDIALS CVODE[21] solver using the backward differentiation formula method. The absolute and the relative error tolerance were 10^{-8} and 10^{-5}, respectively.

RESULTS AND DISCUSSION

Dynamics of Landolt Type Systems in a CSTR. The CSTR content has two stable stationary states (Figure 1). One is characterized with low extent of reaction R2; it is called F_{cstr} state. The other one is called the T_{cstr} state because in this case the extent of reaction R2 is high. In this state at least one of the reactants is nearly totally consumed, in this case A^- because we limit ourself to an excess of B ($b_0 = 1.5$). Bistability appears in a wide range of κ_2, as shown in Figure 2. As κ_2 increases, the limits of the stability of the stationary states shift to lower h_0, in agreement with the experimental observations. Because bromate is a sluggish oxidant, in experiments with the BS system the typical range of the acid input flow concentration is 1−10 mM, whereas in the case of the HPS reaction due to the faster oxidation of the sulfite ions by hydrogel peroxide, it is about 10 times smaller. In the presence of the second-order term, at nonzero κ_2', the limit of the F_{cstr} is shifted to lower h_0, whereas that of the T_{cstr} is nearly unaffected. That means the second-order term has a significant contribution at high pH, e.g., when the CSTR content belongs to the F_{cstr} state, but it is overcast by the third-order one at lower pH. Hereafter, we study the dynamics of the gel content only, when the CSTR is maintained at the F_{cstr} state; consequently, the gel is fed by an almost unreacted mixture of the chemicals.

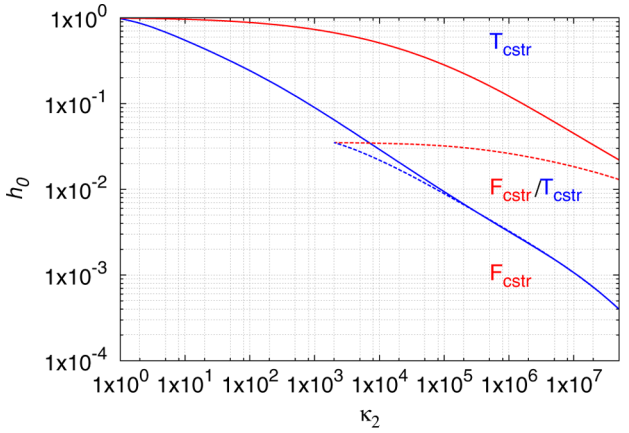

Figure 2. Phase diagram of the CSTR content in the κ_2−h_0 plane at $\kappa_2' = 0$ (solid lines) and at $\kappa_2' = 50$ (dashed lines).

Dynamics of Landolt Type Systems in an OSFR. We start with the general situation where both the second- and the third-order terms are present and the diffusion coefficient of the hydrogen ions is unaffected by weak electrolytes. The values of κ_2, κ_2', and δ are set to 5×10^5, 50, and 1/9, respectively. In this case two different stationary states can develop in the gel (Figure 3) and coexist at a finite range of parameters. This corresponds to spatial bistability. For the F state of the gel content, all the concentration profiles are nearly flat: even at the furthermost point ($x = l_x$) the values of the variables are close to the feeding ones, e.g., $h(x = l_x) \approx h_{cstr}$. At the M state of the gel content a sharp chemical front arises at finite distance from the feeding surface as a result of the autocatalytic process. Behind the front a and a^h decrease, while h increases. The profile of b in the M state does not differ significantly from that in the F state, due to the excess of B.

Besides the stationary states, two different type of oscillations can emerge (Figure 4) at appropriate conditions. When the F state becomes unstable, periodical changes between high and

dx.doi.org/10.1021/jp508836p | J. Phys. Chem. A 2014, 118, 10699−10705

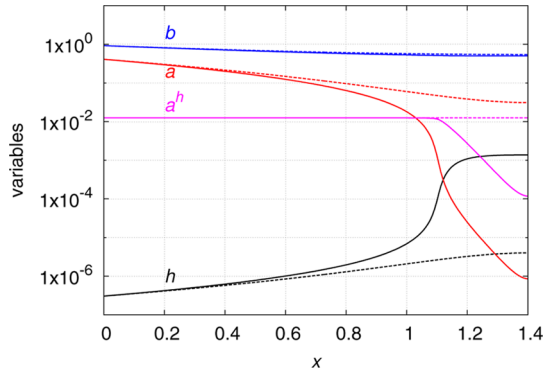

Figure 3. Stable concentration profiles in the gel along axis x at $l_x = 1.4$ and $h_0 = 0.0125$. The dashed and solid lines show the profiles at the F and M states, respectively. The parameters are $\kappa_1 = 5 \times 10^{10}$, $\kappa_{-1} = 5 \times 10^5$, $\kappa_2 = 5 \times 10^5$, $\kappa_2' = 50$, and $\delta = 1/9$.

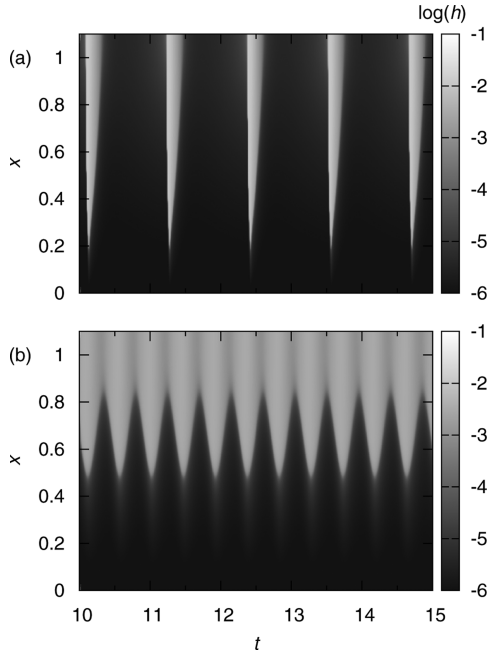

Figure 4. Time−space plots of the two oscillatory states F′ (a) and M′ (b) at $l_x = 1.1$ and $h_0 = 0.018$. The other parameters are the same as in Figure 3.

low values of h develop everywhere along x (Figure 4a), except in a tiny region near the feeding surface ($x \sim 0$). We call it the F′ state of the gel content. For the M′ state relatively small amplitude concentration oscillations form in the inner part of the gel (Figure 4a), while close to the feeding surface the gel content stays in a low ξ value state. These two zones are connected through a region where the position of the autocatalytic front moves back and forth along the x axis. The appearance of these multiple types of spatiotemporal oscillations have been observed experimentally in the IS reaction and supported by numerical simulations by using a specific kinetic model.[15]

Here, we use two control parameters, the thickness of the gel (l_x) and the input feed concentration of the autocatalytic species (h_0) to describe the dynamics of the system (Figure 5). The state of the system is sensitive for these parameters and both can be used to scan the spatiotemporal behavior of the gel content. The maximum value of h_0 is limited, because the F_{cstr} is

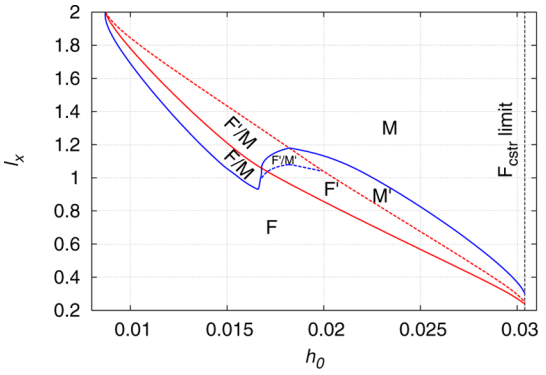

Figure 5. Nonequilibrium phase diagram of the gel content in the h_0−l_x parameter plane. Here, F, M, F′, and M′ denote the two stationary spatial states and the two type of spatiotemporal oscillations, respectively. The other parameters are the same as in Figure 3.

stable up to $h_0 = 0.304$, for the conditions used here. The phase diagram in Figure 5 shows that bistability is favored at large values of l_x, whereas oscillations are preferred at low values. To present the dynamics of the system, bifurcation diagrams are taken at representative values of l_x, where the $h(x=l_x)$ are plotted against the control parameter h_0. At $l_x = 1.4$ (Figure 6a)

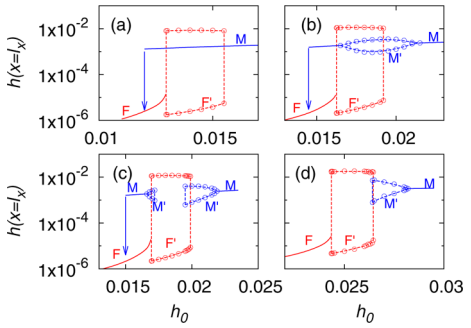

Figure 6. Bifurcation diagrams at $l_x = 1.4$ (a), $l_x = 1.1$ (b), $l_x = 1.05$ (c), and $l_x = 0.6$ (d). The red and blue solid lines denote the F and M states. The red and blue dashed lines with circles indicate the amplitude of the oscillations.

starting at $h_0 = 0.011$ the F state is the only stable state of the system. When h_0 is increased, this state is stable up to $h_0 = 0.01294$. By a further increase of h_0, large amplitude F′ oscillations appear with finite amplitudes. The F′ state is stable up to $h_0 = 0.0155$, where the system jumps to the M state. Now, with decreasing h_0, the M state is stable until $h_0 = 0.0120$. By a further decrease of h_0, the system jumps back to the F state.

At $l_x = 1.1$ (Figure 6b) a new instability comes into play. The F state is stable until $h_0 = 0.0162$, where now F′ oscillations appear. At $h_0 = 0.0193$ a sharp transition from the F′ to the M′ oscillations can be observed. Now, starting at the M state, e.g., at $h_0 = 0.230$, by deceasing h_0 the M state becomes unstable for M′ oscillations at $h_0 = 0.0215$, with a smooth increase of amplitude (supercritical Hopf bifurcation). The M′ is stable until $h_0 = 0.0165$, where the system smoothly returns to the M state. The back-transition from the M to the F state appears at $h_0 = 0.0145$. The stability ranges of the F′ and the M′ states overlap; thus the system shows birhythmicity. The time−space plots in Figure 4 show the two type of oscillations develop for the same conditions.

dx.doi.org/10.1021/jp508836p | J. Phys. Chem. A 2014, 118, 10699−10705

At slightly lower thickness parameter, l_x = 1.05 (Figure 6c), the situation becomes even more complex. Similarly to the previous case, starting from the monostable F state and by increasing h_0, first the F′ oscillations can be reached and at h_0 = 0.0199 there is a sharp switch to the M′ oscillations. Over this range of parameters, when h_0 is decreased, the M′ oscillations become unstable at h_0 = 0.0195 and the system jumps back to the F′ oscillations. By a further decrease of h_0, F′ to F transition occurs. However, between 0.0150 < h_0 < 0.0166 not only the F or the F′ states are stable but also there is an island of the M and the M′ states, which cannot be reached by changing h_0, but by a finite spatial perturbation.

Finally, at l_x = 0.6 (Figure 6d), when h_0 is moved back and forth, F ↔ F′ ↔ M′ ↔ M bifurcation sequences are found. Contrary to the above cases, there is no hysteresis in the transition between the F′ and M′ oscillations, but it occurs through a sequence of mixed mode oscillations. A large amplitude oscillation is followed by increasing the number of low amplitude ones (Figure 7a−c). Using a L^S notation, where

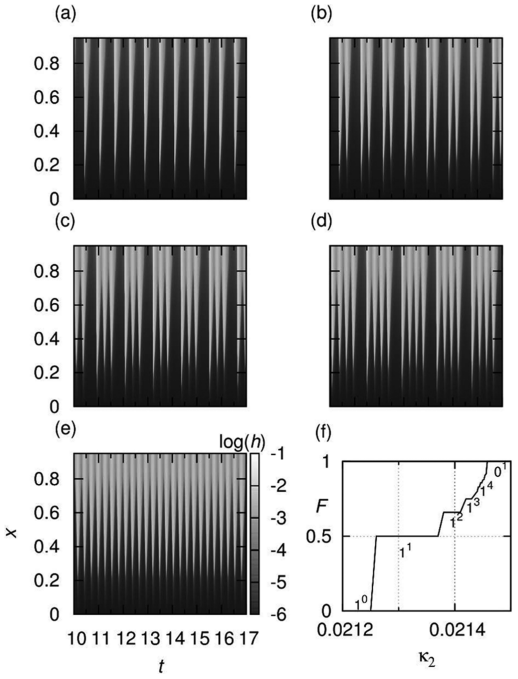

Figure 7. Time−space plots of the transition from the F′ (a) to M′ (e) state through mixed mode oscillations: 1^1 (b), 1^2 (c), and 1^3 (d), at increasing values of h_0 (0.0212, 0.02130, 0.02140, 0.02142, 0.02146) at l_x = 0.95 (e) and the firing number as a function of h_0 (f).

L and S are the numbers of large and small amplitude oscillations, the observed sequence is 1°,1^1,1^2,...,1^{11},0^1. This dynamics can be represented by using the firing number, which is defined as $F = S/(L + S)$. On the plot of F as a function of the h_0 staircase, any range of the same L^S pattern gives rise to a step on this staircase (Figure 7d). A similar alternation between two spatiotemporal oscillatory modes has also been observed experimentally in the IS reaction operated in an OSFR.[9]

To understand the origin of the dynamical complexity of this system, we have consecutively studied the role first played by the kinetics of reaction R2, and then by the difference in the diffusivity of species.

Role of the Kinetics of the Autocatalysis. We start at a thickness where both types of oscillations can be observed, e.g., l_x = 0.6, and use h_0 and κ_2' as control parameters. The computed phase diagram is shown in Figure 8. As κ_2' decreases, the limit of

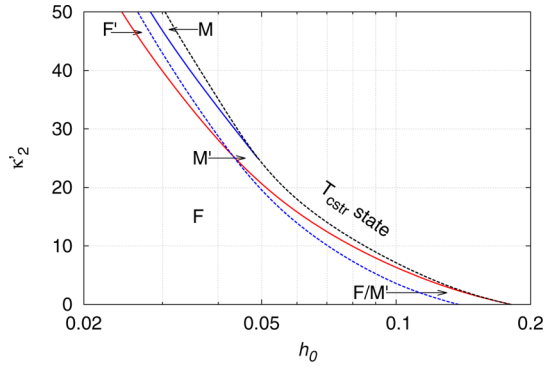

Figure 8. Nonequilibrium phase diagram of the gel content in the h_0−κ_2' parameter plane at l_x = 0.6.

the F_{cstr} shifts to higher h_0 and the limit of the M′ state moves in parallel. Consequently, the relative width of the parameter range over the M′ oscillations does not change significantly. However, both the F′ and the M states disappear as κ_2' decreases. Around κ_2' = 25 the stability limit of the M state hits that of the F_{cstr}. At the same parameter value, the domain of F′ oscillations vanishes. The topology of the phase diagram is reminiscent of the standard cross shaped one:[22,23] below a critical value of κ_2', there is bistability between the F and M′ states, and above it, the domains of these states are separated by that of the F′ oscillations.

Let us compare again the bifurcation diagrams at $x = l_x$. The starting point corresponds to Figure 6d, where κ_2' = 50 and a F ↔ F′ ↔ M′ ↔ M bifurcation sequence is found. At κ_2' = 25 (Figure 9a), the h_0 parameter range of F′ oscillations and the M

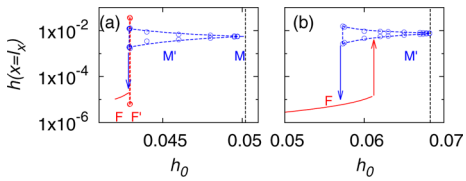

Figure 9. Bifurcation diagrams at κ_2' = 25 (a) and κ_2' = 15 (b). The red and blue solid lines denote the F and M states. The red and blue dashed lines with circles indicate the amplitude of the oscillations.

state become vary narrow, whereas at κ_2' = 15, only the F and the M′ s exist, and their range of stability overlaps, thus bistability between these states can be seen. The most important conclusion is that the appearance of F′ oscillations is found only above a critical value of the second-order kinetic term (κ_2').

In the vicinity of the F ↔ M′ transition, complex and even chaotic spatiotemporal oscillations develop, as shown in Figure 10. Starting at h_0 = 0.0595 (Figure 10a), simple oscillations form. By changing to h_0 = 0.0585, one can see period doubling (Figure 10b), whereas at h_0 = 0.0575, the oscillations become chaotic (Figure 10c). The chaotic nature of these oscillations is revealed by calculating a Lorenz map from a time series data collected along a selected position, e.g., x = 0.15 (Figure 10d). This one-dimensional map shows the N + 1 maximum of $h(x$=0.15) as a function of N maximum of $h(x$=0.15).

dx.doi.org/10.1021/jp508836p | J. Phys. Chem. A 2014, 118, 10699−10705

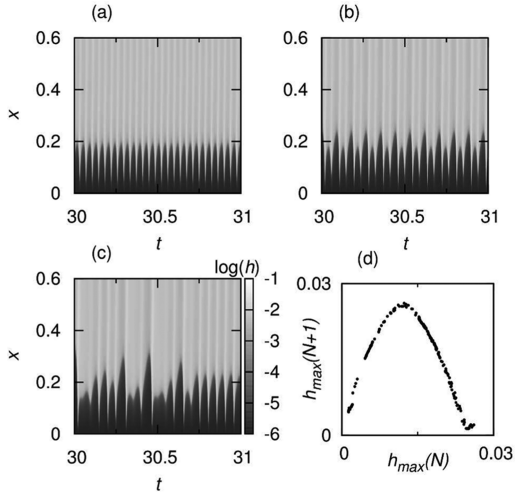

Figure 10. Time−space plots of the transition from simple to chaotic oscillations: h_0 = 0.0595 (a), h_0 = 0.0585 (b), and h_0 = 0.0575 (c) at l_x = 0.6 and κ_2' = 15. (d) Lorenz map calculated from the time series data collected at h_0 = 0.575 along the position x = 0.15.

Essential Ingredient: Long-Range Activation. At last, we explore the effect of parameter δ, which accounts for the relative diffusivity of the hydrogen ions compared to the case of the other species, in ranges of other parameters where both types of oscillations exist (l_x = 0.6 and κ_2' = 50). This allows us to study the role of long-range activation on the dynamics of the system. In the absence of weak electrolytes we can assume that hydrogen ions diffuse 9 time faster that the other ions, thus δ = 1/9. However, in the presence of any compounds that bind hydrogen ions, δ is larger than that. The effective diffusivity of the hydrogen ions is affected by the substrate A, but this influence is accounted for in the model by reaction R1. The variation of the value of δ corresponds to the presence of additional weak electrolytes, like the carboxylic functions of the gel matrix or the applied pH indicator in the experiments. The actual value of δ depends on the concentrations, on the pK_a values, and on the diffusion coefficients of these weak electrolytes.

The calculated phase diagram (Figure 11) shows a cross-shaped topology;[22,23] as δ increases, both types of oscillations disappear, and below a critical value of δ, steady-state bistability between the F and M can be found. This phase diagram demonstrates that differential diffusion is a prerequisite of the rich spatiotemporal dynamics of Landolt type systems, because

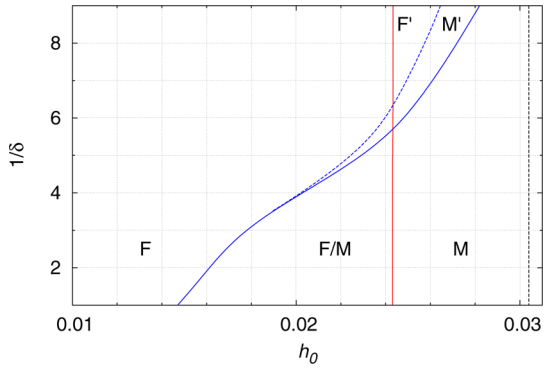

Figure 11. Nonequilibrium phase diagram of the gel content in the h_0−δ parameter plane at l_x = 0.6 and κ_2' = 50.

it provides the necessary negative feedback. The development of both types of oscillations requires a low value of δ, typical lower than 1/5. These results are in good agreement with the previous experimental observations[17] and also with the theoretical studies.[12−14,16]

CONCLUSION

Our numerical simulations point out that Landolt type autocatalytic systems are capable of showing a large variety of spatiotemporal behaviors, e.g., spatial bistability, oscillations, birhythmicity, mixed mode, and chaotic oscillations, in an OSFR. In contrast, in a spatially homogeneous reactor with equal residence time for all species, e.g., in a CSTR, these reactions can produce only steady-state bistability. In the OSFR the positive feedback is provided by the chemistry, whereas the negative one is the result of the differences in the transport properties of the chemicals. The relatively fast diffusive escape of the autocatalytic species from the gel compared to the exchange of the other species is an essential ingredient of the system. The kinetic properties of the autocatalytic reaction R2, namely, the presence of second- and third-order terms in its rate law, have also significant contribution to this rich dynamics. Due to these two terms two different types of oscillations can develop and the interaction of these oscillatory modes results in the appearance of mixed mode and chaotic oscillations. Notably, complex oscillations have been already experimentally observed in the IS reaction.[9] Our numerical simulations suggest that F′ oscillations develop only in the presence of the second-order term. It would be a challenging problem to prove this connection by using some kind of analytical method. In addition, in the CT reaction only M′ type oscillations have been found both in the experiments and in the corresponding simulations only. The rate law of this superautocatalytic reaction can be written as $v = k[A][B][H^+]^2$, where A and B are tetrathionate and chlorite, respectively. This points again to the fact that M′ type oscillations are preferred in systems with higher-order nonlinearity.

Among the Landolt type systems long-range activation oscillations have been observed only in the IS reaction,[9] although both the BS and the HPS reaction have been studied in OSFR.[10,11] Considering the kinetics of these analogous reactions significant differences can be found in the rate constants (k_2 and k_2') of the oxidation step (R2) and due to the presence of different additional reaction steps. However, the differences in the rate constants can be compensated by adjusting the input feed concentrations and the residence time of the CSTR, according to the dimensionless parameters, e.g., $\kappa_2 = k_2[A]_0^2/k_0$. The significance of the side reactions depend on the actual conditions, e.g., on the ratio of the oxidant and sulfite concentrations, but there are conditions at which the general model, including reactions R1 and R2, provide a reasonable description of the kinetics. Accordingly, we can assume that Landolt type reactions independent from the nature of the oxidant are capable of showing long-range activation oscillations and other spatiotemporal phenomena under appropriate conditions. However, there are important factors that might limit the experimental observations, especially δ and l_x. To reach appropriately low values of δ, it is suggested to keep the amount of the weak electrolytes (pH indicator, gel , etc.) as low as possible in the reacting mixture. It can be also difficult to find the proper thickness (l_x), but a nice method, the use of conical shape gel have been suggested by De Kepper for this express purpose.[17]

dx.doi.org/10.1021/jp508836p | J. Phys. Chem. A 2014, 118, 10699−10705

The dynamics of Landolt systems can be enriched by introducing a negative feedback trough an additional reaction. This was effectively used to design pH oscillators, which are capable of showing large amplitude periodic changes in the pH of a CSTR content.[24] In these systems both the activatory and the inhibitory processes are provided by chemical reactions. Interestingly, mixed mode[25] and chaotic[26] oscillations in a CSTR could also be generated in pH oscillators. These extended Landolt systems have been found to be capable of showing various nontrivial spatiotemporal behavior in OSFR, including waves, stationary patterns, and self-replicating patterns.[11,27−32] However, the possible interaction of long-range activation and a negative feedback induced by a chemical reaction have not been studied either experimentally or theoretically. We believe that Landolt systems, although they date back to the 19th century, still provide an interesting area for further studies.

AUTHOR INFORMATION

Corresponding Author

*E-mail: szalai.istvan@chem.elte.hu.

Notes

The authors declare no competing financial interest.

ACKNOWLEDGMENTS

The author thanks Patrick De Kepper for fruitful discussions. We acknowledge the support from the Hungarian Research Fund (100891).

REFERENCES

(1) Epstein, I. R.; Pojman, J. *An Introduction to Nonlinear Chemical Dynamics*; Oxford University Press: New York, 1988.

(2) Nagypal, I.; Epstein, I. R. Fluctuations and Stirring Rate Effects in the Chlorite-Thiosulfate Reaction. *J. Phys. Chem.* **1986**, *90*, 6285−6292.

(3) Landolt, H. Ueber die Zeitdauer der Reaction zwischen Jodsäure und schwefliger Säure. *Ber. Dtsch. Chem. Ges.* **1886**, *19*, 1317−1365.

(4) Edblom, E. C.; Luo, Y.; Orban, M.; Epstein, I. R. Systematic Design of Chemical Oscillators. 45. Kinetics and Mechanism of the Oscillatory Bromate-Sulfite-Ferrocyanide Reaction. *J. Phys. Chem.* **1989**, *93*, 2722−2727.

(5) Rábai, G.; Kustin, K.; Epstein, I. R. A Systematically Designed Ph Oscillator: The Hydrogen Peroxide-Sulfite-Ferrocyanide Reaction in a Continuous-Flow Stirred Tank Reactor. *J. Am. Chem. Soc.* **1989**, *11*, 3870−3874.

(6) Blanchedeau, P.; Boissonade, J. Resolving an Experimental Paradox in Open Spatial Reactors: The Role of Spatial Bistability. *Phys. Rev. Lett.* **1998**, *81*, 5007.

(7) Borckmans, P.; Benyaich, K.; Dewel, G. Spatial Bistability: A Chemical Idiosyncrasy? *Int. J. Quantum Chem.* **2004**, *98*, 239−247.

(8) Boissonade, J.; Dulos, E.; Gauffre, F.; Kuperman, M. N.; De Kepper, P. Spatial Bistability and Waves in a Reaction with Acid Autocatalysis. *Faraday Discuss.* **2002**, *120*, 353−361.

(9) Szalai, I.; De Kepper, P. Spatial Bistability, Oscillations and Excitability in the Landolt Reaction. *Phys. Chem. Chem. Phys.* **2006**, *8*, 1105−1110.

(10) Virányi, Z.; Szalai, I.; Boissonade, J.; De Kepper, P. Sustained Spatiotemporal Patterns in the Bromate-Sulfite Reaction. *J. Phys. Chem. A* **2007**, *111*, 8090−8094.

(11) Szalai, I.; Horváth, J.; Takács, N.; De Kepper, P. Sustained Self-Organizing pH Patterns in Hydrogen Peroxide Driven Aqueous Redox Systems. *Phys. Chem. Chem. Phys.* **2011**, *13*, 20228−20234.

(12) Fuentes, M.; Kuperman, M. N.; Boissonade, J.; Dulos, E.; Gauffre, F.; De Kepper, P. Dynamical Effects Induced by Long Range Activation in a Nonequilibrium Reaction-Diffusion System. *Phys. Rev. E* **2002**, *66*, 056205.

(13) Benyaich, K.; Erneux, T.; Metens, S.; Villain, S.; Borckmans, P. Spatio-Temporal Behaviors of a Clock Reaction in an Open Gel Reactor. *Chaos* **2006**, *16*, 037109.

(14) Szalai, I. Linear Diffusive Feed Approach to Explaining Long Range Activation Induced Oscillations. *React. Kinet. Mech. Catal.* **2014**, *111*, 431−442.

(15) Boissonade, J.; De Kepper, P. Multiple Types of Spatio-Temporal Oscillations Induced by Differential Diffusion in the Landolt Reaction. *Phys. Chem. Chem. Phys.* **2011**, *13*, 4132−4137.

(16) Szalai, I.; Gauffre, F.; Labrot, V.; Boissonade, J.; De Kepper, P. Spatial Bistability in a pH Autocatalytic System: From Long to Short Range Activation. *J. Phys. Chem. A* **2005**, *109*, 7843−7849.

(17) Labrot, V.; Hochedez, A.; Cluzeau, P.; De Kepper, P. Spatiotemporal Dynamics of the Landolt Reaction in an Open Spatial Reactor with Conical Geometry. *J. Phys. Chem. A* **2006**, *110*, 14043−14049.

(18) Bánsági, T., Jr.; Taylor, A. F. Role of Differential Transport in an Oscillatory Enzyme Reaction. *J. Phys. Chem. B* **2014**, *118*, 6092−6097.

(19) Molnár, I.; Takács, N.; Kurin-Csörgei, K.; Orbán, M.; Szalai, I. Some General Features in the Autocatalytic Reaction between Sulfite Ion and Different Oxidants. *Int. J. Chem. Kinet.* **2013**, *45*, 462−468.

(20) Rábai, G. Modeling and Designing of pH-Controlled Bistability, Oscillations, and Chaos in a CSTR. *ACH - Models Chem.* **1998**, *135*, 381−392.

(21) Hindmarsh, A. C.; Brown, P. N.; Grant, K. E.; Lee, S. L.; Serban, R.; Shumaker, D. E.; Woodward, C. S. SUNDIALS: Suite of Nonlinear and Differential/Algebraic Equation Solvers. *ACM Transactions on Mathematical Software* **2005**, *31*, 363−396.

(22) Boissonade, J.; De Kepper, P. Transitions from Bistability to Limit Cycle Oscillations. Theoretical Analysis and Experimental Evidence in an Open Chemical System. *J. Phys. Chem.* **1980**, *84*, 501−506.

(23) Dangelmayr, G.; Guckenheimer, J. On a Four Parameter Family of Planar Vector Fields. *Arch Ration. Mech. Anal.* **1987**, *97*, 321−352.

(24) Rábai, G.; Orbán, M.; Epstein, I. R. Systematic Design of Chemical Oscillators. 64. Design of pH-Regulated Oscillators. *Acc. Chem. Res.* **1990**, *23*, 258−263.

(25) Bakes, D.; Schreiberová, L.; Schreiber, I.; Hauser, M. J. B. Mixed-Mode Oscillations in a Homogeneous pH-Oscillatory Chemical Reaction System. *Chaos* **2008**, *18*, 015102.

(26) Rábai, G.; Hanazaki, I. Chaotic pH Oscillations in the Hydrogen Peroxide-Thiosulfate-Sulfite Flow System. *J. Phys. Chem. A* **1999**, *103*, 7268−7273.

(27) Lee, K. J.; McCormick, W. D.; Ouyang, Q.; Swinney, H. L. Pattern Formation by Interacting Chemical Fronts. *Science* **1993**, *261*, 192−194.

(28) Lee, K. J.; McCormick, W. D.; Pearson, J. E.; Swinney, H. L. Experimental Observation of Self-Replicating Spots in a Reaction-Diffusion System. *Nature* **1994**, *369*, 215−218.

(29) Szalai, I.; De Kepper, P. Patterns of the Ferrocyanide-Iodate-Sulfite Reaction Revisited: The Role of Immobilized Carboxylic Functions. *J. Phys. Chem. A* **2008**, *112*, 783−786.

(30) Horváth, J.; Szalai, I.; De Kepper, P. An Experimental Design Method Leading to Chemical Turing Patterns. *Science* **2009**, *324*, 772−775.

(31) Liu, H.; Pojman, J. A.; Zhao, Y.; Pan, C.; Zheng, J.; Yuan, L.; Horváth, A. K.; Gao, Q. Pattern Formation in the Iodate-Sulfite-Thiosulfate Reaction-Diffusion System. *Phys. Chem. Chem. Phys.* **2012**, *14*, 131−137.

(32) Molnár, I.; Kurin-Csörgei, K.; Orbán, M.; Szalai, I. Generation of Spatiotemporal Calcium Patterns by Coupling a pH-Oscillator to a Complexation Equilibrium. *Chem. Commun.* **2014**, *50*, 4158−4160.